Increasing the density in Wendelstein 7-X: Benefits and limitations

G. Fuchert[1,*], K.J. Brunner[1], K. Rahbarnia[1], T. Stange[1], D. Zhang[1], J. Baldzuhn[1], S.A. Bozhenkov[1], C.D. Beidler[1], M.N.A. Beurskens[1], S. Brezinsek[2], R. Burhenn[1], H. Damm[1], A. Dinklage[1], Y. Feng[1], P. Hacker[1], M. Hirsch[1], Y. Kazakov[3], J. Knauer[1], A. Langenberg[1], H.P. Laqua[1], S. Lazerson[1], N.A. Pablant[4], E. Pasch[1], F. Reimold[1], T. Sunn Pedersen[1], E.R. Scott[1], F. Warmer[1], V.R. Winters[1,5], R.C. Wolf[1,6] and W7-X Team

[1] Max-Planck-Intitut für Plasmaphysik, Greifswald, Germany

[2] Forschungszentrum Jülich, Jülich, Germany

[3] Royal Military Academy, Brussels, Belgium

[4] Princeton Plasma Physics Laboratory, Princeton, NJ, USA

[5] University of Wisconsin-Madison, Madison WI, USA

[6] Technische Universität Berlin, Berlin, Germany

1 Abstract

In stellarators, increasing the density is beneficial for the energy confinement. While there is no single reason for this observation, it is still very robust across different devices and this is reflected in the empirical energy confinement time scaling for stellarators, ISS04. In order to study whether this is also true for Wendelstein 7-X, the density scaling of the energy confinement time is analyzed and compared to ISS04 for the first divertor experiments. When the density is increased beyond a critical density, however, radiative collapses are frequently observed. Existing analytical models for the critical density are revisited to assess whether they can predict the accessible density range. Furthermore, since close to the collapse the radiation losses increase substantially, the impact on the global energy confinement is investigated. It is found that in plasmas with high radiation the density scaling of the energy confinement time becomes weaker, the reason for this observation is not yet clear. In the second half of the first divertor campaign, boronization was applied to W7-X for the first time. This broadened the operational window, allowing for operation at higher density and, hence, higher stored energy.

2 Introduction

Both in tokamaks and stellarators high-density (on the order of $10^{20}\,\mathrm{m}^{-3}$) operation is mandatory for achieving high fusion performance. As the first comprehensively optimized stellarator, Wendelstein 7-X (W7-X) is an essen-

* golo.fuchert@ipp.mpg.de

tial experiment to study the benefits and limits of increasing the density in this kind of device. This includes investigations of the density dependence of the energy confinement and limitations of the achievable density. Theoretical predictions and empirical scaling laws for the energy confinement time, τ_E, in stellarators (e.g. the ISS04 scaling [1]) predict a positive correlation between the plasma density and the energy confinement time. This suggests that higher densities in fusion plasmas could be beneficial for the triple product $nT_\mathrm{i}\tau_\mathrm{E}$, since a decreasing temperature should be overcompensated by the increase of the energy confinement time and the density itself, and before equipartition (electron temperature T_e equal to the ion temperature T_i) even the ion temperature itself may increase with density due to an increased coupling of the two species. Since this line of argument is only valid as long as fusion-relevant temperatures can be sustained and only in parameter regimes where the density scaling of τ_E is indeed positive, experimental evidence is particularly important close to operational limits or changing confinement regimes. This leads to the rather obvious conclusion that the energy confinement time scaling and the presence of operational limits and different confinement regimes have to be understood and studied as an intertwined system. While this is already a common approach in tokamak research, it is still an open issue for stellarators. The reasons are the lack of an extensive set of large experimental devices (with only LHD [2] being comparable in size to W7-X) and the fact that different field configurations may show substantial differences.

The experimental exploitation of W7-X has only started. However, the gradual completion of the machine capabilities [3] (especially concerning the installation of the high-heatflux divertor and the completion of heating capabilities) are an ideal opportunity to map out the configuration space accessible in the current configuration and to identify key issues on the route to high-performance long-pulse operation. So far, experiments in W7-X have been conducted in a limiter configuration in the experimental campaign called OP1.1 [4–6] and in a test-divertor configuration in OP1.2 (which was divided in two halves, OP1.2a and OP1.2b; see Refs. [7, 8] for more details). One of the obstacles in these early experiments was the frequent occurrence of radiative collapses terminating plasma operation. In such a collapse, the radiated power exceeds the heating power, leading to a sudden decrease of the stored energy. The general phenomenon of radiative collapses is commonly observed in many stellarators and is usually attributed to impurity radiation. While the exact dynamics of the collapse can be very different depending on the temperature profile and the impurity species present in the plasma [9], two main reasons can be distinguished: Either the impurity concentration in the plasma or the radiated power per impurity particle increases. The latter

typically occurs at low plasma temperatures, where the radiative cooling coefficient is increasing with decreasing temperature (for light impurities like carbon and oxygen the relevant temperature range for this is a few hundred eV). If this happens only locally, it can lead to formation of a Marfe [10], which has also been observed in W7-X [11]. In both cases, the stored energy decreases close to the collapse since a large fraction of the heating power is lost as radiation and is, therefore, not available to the plasma. Furthermore, since at constant heating power an increase in density leads to a decrease in temperature (and hence an even stronger radiative cooling), a critical density arises, at which the radiative collapse is triggered. In the literature, this is often referred to as the density limit, radiative density limit or Sudo-limit [12] of stellarators. It is important to note, however, that this is an operational density limit, meaning that the experimental scenario and wall conditions can be adapted (within limitations) to achieve higher densities. Two common strategies to increase the density further (at constant heating power) are pellet fueling and advanced wall-conditioning methods such as boronization.

Nevertheless, these radiative collapses limit the accessible operational space of a stellarator and possibly degrade energy confinement in operational regimes close to the critical density. In the limiter campaign of W7-X, OP1.1, the energy confinement time followed approximately the empirical ISS04 scaling for stellarators [1]:

$$\tau_{\mathrm{ISS04}} = 0.134 \cdot a^{2.28} R^{0.64} P^{-0.61} n_{\mathrm{e}}^{0.54} B^{0.84} \iota_{2/3}^{0.41} \,, \tag{1}$$

Here, a and R are the minor and major radii in meters, P is the heating power in MW, n_{e} the line-averaged electron density in $10^{19}/\mathrm{m}^3$, B the magnetic field strength in T and $\iota_{2/3}$ the rotational transform at 2/3 of the effective radius. At low heating power, it was found that in some experiments radiation dominates the power balance and both the power and density scaling differ strongly from ISS04 [13]. It was, however, not clear if these results could directly be transferred to divertor operation, since the impurity concentrations and spatial distributions could change drastically. Hence, in the following, existing analytical models for the critical density of the radiative density limit are briefly reviewed and applied to W7-X and experimental results of the critical density and the energy confinement time scaling close to it are revisited for the first test-divertor experiments.

3 Analytical models and scaling laws for a critical density

Radiative collapses are commonly observed in stellarators. For a given set of experimental conditions, there is a critical density, n_c, above which the power radiated by the plasma increases abruptly. Eventually, the radiated power exceeds the heating power and the plasma suffers a thermal collapse. The detailed dynamics and onset density of these collapses are heavily dependent on the experimental scenario and machine conditions, especially concerning the type, concentration and spatial distribution of the main impurities. This can, in principle, lead to very complex radiation and collapse dynamics [9]. In most stellarator experiments, however, a few general features are observed relatively robustly: While different fueling, heating and wall conditioning schemes show strong variations in the critical density, in a particular scenario n_c is rather reproducible and increases with the heating power. Often it is observed that the collapse is caused by impurity radiation particularly from the edge of the plasma. The global power balance can be disturbed by an inward-movement of the radiation front, changes in the transport due to the change of the edge profiles or by a loss of heating in case of a pressure-dependent absorption. Experimentally, detailed studies of the evolution of the plasma after the initial onset of the collapse are often hampered by a shutdown initiated by safety systems. In any case the collapse results in an undesired state for a fusion plasma.

Originally, there were two main models that try to predict the critical density. One starts from an analytical 1D power balance equation, ignoring the complex stellarator geometry and all local effects. The scaling law derived from this in [14] reads:

$$n_c = \lambda \frac{P}{a} \,. \tag{2}$$

The factor λ consists of parameters describing the heat transport, radiation characteristics, and field geometry. The second one is a commonly used scaling law, the Sudo density limit, which started as an empirical fit to experimental data [12]:

$$n_{\mathrm{Sudo}} = 0.25 \cdot \sqrt{\frac{PB}{a^2 R}} \,. \tag{3}$$

The most obvious difference between the two equations is the scaling of n_c with the heating power. While Eq. (2) depends linearly on the heating power, Eq. (3) shows a square-root dependence. Later it was discussed that the prefactor λ in Eq. (2) is not a constant and depends, among other quantities, on the heat diffusivity and the impurity density. These quantities are not

necessarily known a priori and in order to obtain a scaling law for the critical density, characteristic average values or scaling laws have to be employed. In Refs. [15, 16] the heat diffusivity was estimated by using scaling laws for the energy confinement time τ_E together with the definition of an effective heat diffusivity $\chi_\mathrm{eff} = a^2/\tau_\mathrm{E}$. Such an approach to estimate the heat transport will of course only result in meaningful predictions for parameter ranges where the τ_E-scaling is valid. Effects like bifurcations or critical-gradients that could arise, for example, from plasma turbulence would require a more careful treatment. In the absence of such effects this leads to the expression

$$n_\mathrm{c} = \frac{P}{4\pi^2 R a} \cdot \sqrt{\frac{\tau_\mathrm{E}}{a^2 n_\mathrm{e}} \frac{c_\mathrm{rad}}{f_\mathrm{imp}}} \,. \tag{4}$$

Here, $f_\mathrm{imp} = n_\mathrm{imp}/n_\mathrm{e}$ is the impurity fraction in the radiation zone (mainly at the edge) and c_rad is a constant describing the simplified radiation model described in [14], where oxygen is assumed as main radiating impurity and $c_\mathrm{rad} = 6.25 \cdot 10^{48}\,\mathrm{W^{-2}m^{-3}s^{-1}}$. Since it is observed in stellarators that τ_E depends on the heating power and density, this leads to a scaling law of the general form

$$n_\mathrm{c} = c \cdot \frac{P^\alpha}{f_\mathrm{imp}^\beta} \,. \tag{5}$$

In Ref. [16] it is shown that the Sudo-limit is a special case of Eq. (5) and, hence, the two models introduced above are essentially identical. In this representation, Eq. (5) assumes that the impurity fraction f_imp is constant for a specific experimental scenario. In the first experimental campaign, OP1.1, line-averaged Z_eff measurements indicated values between 1.5 and 5 (e.g. a value of 3.5 has been reported in [17]) with carbon and oxygen as dominant impurities. Spatially resolved measurements were not available. In OP1.2b, after boronization was available, Z_eff usually was found to be below 2 again with carbon and oxygen as main impurities and initial profile measurements using charge-exchange spectroscopy indicated flat profiles (to be published). Assuming either carbon or oxygen as main (edge) impurity, the impurity fraction can be calculated from Z_eff. For example, a Z_eff of 2 would correspond to $f_\mathrm{imp} = 3.3\,\%$ for carbon and $1.8\,\%$ for oxygen and a Z_eff of 4 to $f_\mathrm{imp} = 10\,\%$ for carbon and $5.4\,\%$ for oxygen (for a single impurity species in a hydrogen plasma it is $Z_\mathrm{eff} = n_\mathrm{H,i}/n_\mathrm{e} + Z_\mathrm{imp}^2 n_\mathrm{imp}/n_\mathrm{e}$ and $n_\mathrm{H,i}/n_\mathrm{e} = 1 - Z_\mathrm{imp} f_\mathrm{imp}$ and, hence, $f_\mathrm{imp} = (Z_\mathrm{eff} - 1)/(Z_\mathrm{imp}^2 - Z_\mathrm{imp})$).

In order to obtain a characteristic scaling, however, the exact choice of f_imp is not too important due to the weak dependence of Eq. (4) on the impurity fraction. Even rough estimates of f_imp will lead to a relatively precise prediction of n_c. When comparing n_c with experimental data, however, this

advantage turns into a disadvantage: Since Eq. (4) depends on $c_{\mathrm{rad}}/f_{\mathrm{imp}}$, the experimentally inferred impurity fraction absorbs the uncertainties in c_{rad}. While the proportionality is retained, f_{imp} will only represent the actual impurity content in the plasma if c_{rad} is known precisely. In the following, a characteristic f_{imp} of 4 % before and below 1 % after boronization seem reasonable initial guesses that can later be compared with the experimental data. The applicability of Eq. (5) depends far more on the role of local effects and systematic influences on f_{imp}, which would change the functional dependence of the critical density on the heating power or magnetic field properties. For example, in the predecessor experiment Wendelstein 7-AS [18], Z_{eff} was a function of the heating power, which led to a rather weak scaling of the critical density with $P^{0.4}$ [15]. Studying such possible influences in W7-X will be an important task for the future. Furthermore, the estimation of the heat transport by the energy confinement time scaling used to obtain Eq. (4) will of course only result in meaningful predictions for parameter ranges where the scaling is valid. Hypothetical effects including bifurcations or critical-gradients that could arise, for example, from plasma turbulence would require a more careful treatment.

In order to estimate the critical density for W7-X, it is assumed that τ_{E} can be expressed as $\tau_{\mathrm{E}} = f_{\mathrm{r}}\tau_{\mathrm{ISS04}}$ (f_{r} is referred to as *configuration factor*, see Sec. 5 for its definition). Plugging this into Eq. (4), the following expression is obtained:

$$\begin{aligned} n_{\mathrm{c}}[10^{19}\,\mathrm{m}^{-3}] &= \left(\frac{1.8\cdot 10^{-4}}{4\pi^2 R a^2}\sqrt{c_{\mathrm{rad}} a^{2.28} R^{0.64} B^{0.84} \iota_{2/3}^{0.41}}\right)^{0.8} \cdot \frac{f_{\mathrm{r}}^{0.4} P^{0.6}}{f_{\mathrm{imp}}^{0.4}} \\ &= c_{\mathrm{conf}} \cdot \frac{f_{\mathrm{r}}^{0.4} P^{0.6}}{f_{\mathrm{imp}}^{0.4}}\,. \end{aligned} \tag{6}$$

As will be shown in Sec. 5, under the current experimental conditions $f_{\mathrm{r}} \approx 0.75$. For the magnetic standard configuration of W7-X ($R = 5.5\,\mathrm{m}$, $a = 0.51\,\mathrm{m}$, $B = 2.41\,\mathrm{T}$, $\iota = 0.9$) it is $c_{\mathrm{conf}} = 0.56$, for the high-mirror configuration ($R = 5.5\,\mathrm{m}$, $a = 0.5\,\mathrm{m}$, $B = 2.35\,\mathrm{T}$, $\iota = 0.9$) $c_{\mathrm{conf}} = 0.57$, and for the high-iota configuration ($R = 5.5\,\mathrm{m}$, $a = 0.5\,\mathrm{m}$, $B = 2.39\,\mathrm{T}$,$\iota = 1.1$) $c_{\mathrm{conf}} = 0.59$ (details about the different configurations are found in [19]). Hence, there are only small changes in the pre-factor of less than 10 % and no strong variations are expected for n_{c} between the different magnetic configurations foreseen for W7-X. Of course, simple analytical scaling laws cannot predict either f_{imp}, which may vary for the different configurations (e. g. due to different plasma-wall interaction), or local effects due to the complex stellarator geometry including islands. Furthermore, since the described models assume that the radiative losses are dominated by edge radiation, using the

line-averaged density as indicative quantity is only a good approximation if the profile shape is unchanged, which is not necessarily true for all operational regimes and magnetic configurations. This can be accounted for by introducing a shape factor δ connecting the edge density and the line-averaged density. With this Eq. (5) then reads

$$n_\mathrm{c} = c \cdot \delta \cdot \frac{P^\alpha}{f_\mathrm{imp}^\beta} \,. \tag{7}$$

4 Comparison of the critical density with experimental results

Experimental results from the first test divertor campaign OP1.2 are presented and compared to the predicted critical density. For this comparison, gas-puff fueled hydrogen (H) plasmas with ECR heating were selected. In OP1.2, first experiments were also performed with NBI heating and pellet fueling. Both systems were, however, not yet ready for steady-state operation and resulted in transient plasma conditions which are not suitable for a meaningful comparison, yet. In the first phase of the campaign, OP1.2a, boronization was not yet available, while in OP1.2b a direct comparison before and after boronization was possible. In the following, the term radiative collapse is used to describe a plasma state in which the total radiated power exceeds the heating power (according to the bolometry diagnostic described in [20]) and the time derivative of the diamagnetic energy becomes negative. The critical density is determined as the lowest density in an experiment at which these conditions are met. This definition leads to an uncertainty in the question whether a given density is critical or not. On the one hand, for an unsustainably high density the radiated power may still be increasing after the heating power has changed or the experiment ends before the actual collapse. On the other hand, especially after a power step-down, the plasma may still be settling into a new equilibrium while fulfilling the two criteria introduced above. Furthermore, in experiments with continuous fueling ("density ramp experiments") the density, the diamagnetic energy and the radiated power are all evolving quantities and the exact density at which $P_\mathrm{rad} > P_\mathrm{ECRH}$ and $\mathrm{d}W/\mathrm{d}t < 0$ may not be exactly the critical one. This is illustrated by an example density ramp experiment shown in Fig. 1.

The clearest experiment to check whether a given density is critical or not is to choose a constant density and heating power and wait until $\mathrm{d}W/\mathrm{d}t$ and $\mathrm{d}P_\mathrm{rad}/\mathrm{d}t$ either settle to zero or until a radiative collapse occurs. In OP1.2 this approach was, however, not feasible due to the large amount of

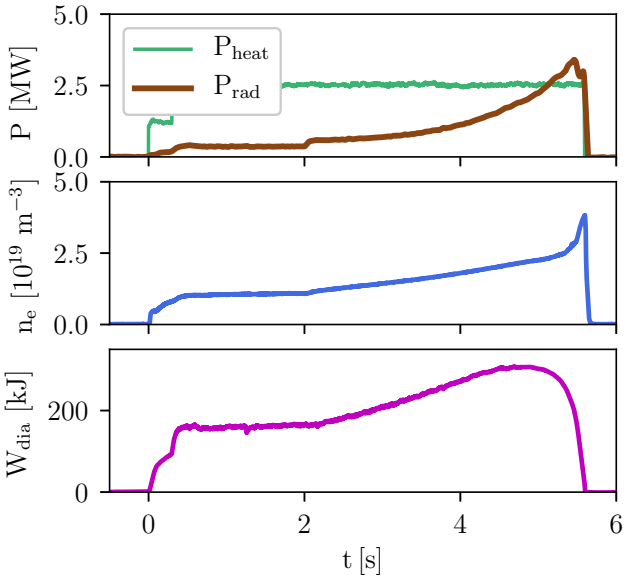

Figure 1: Time traces of the heating power, P_{heat}, the radiated power P_{rad}, the line-averaged density, $\bar{n}_{\mathrm{e}}$, and the diamagnetic energy, W_{dia}, for a density ramp experiment before boronization, ending in a radiative collapse. The evaluated critical density is shown as dashed grey line.

required experimental runtime. In order to tackle this issue, the critical densities found from power step-down experiments without external fueling and density ramp experiments have been compared and no significant difference has been observed so far, suggesting that the variations due to changing machine conditions are larger than the introduced uncertainties due to the experimental definition of the critical density.

4.1 Operation before boronization

The experimental results from OP1.2a and the pre-boronization phase of OP1.2b are shown in Fig. 2. Obviously, the critical density is comparable for both data sets, which demonstrates that the radiative collapse is a robust and reproducible feature. Furthermore, the experimental n_c agrees well with Eq. (6) for low heating power (assuming $f_{imp} = 4\,\%$), but scales more weakly with the heating power than expected. However, the scatter in the data is large (factor of about 1.5), which indicates that the machine conditions may play a significant role in determining the critical density. As a second reference, a curve for $f_{imp} = 20\,\%$ is shown, which is likely too high but matches the collapses at the lowest densities. For fully ionized carbon or oxygen such a high value would not be possible, which points to an issue with the analytical scaling laws: Since the dependence of Eq. (6) on f_{imp} is relatively weak, inaccuracies or incorrect assumptions in the calculation of the prefactors lead to strong variations in the required f_{imp} to match experimental data of the critical density. Possible reasons for the large scatter could be profile or local effects due to the complex stellarator geometry or the existence of a regime with strongly increased impurity influx. It will be shown below (Sec. 4.2) that profile effects (the relationship between the line-averaged and the edge density) are at least one important cause for the observed scatter.

Common ways to achieve higher densities in other stellarator experiments are sophisticated wall conditioning or fueling techniques like, for example, boronization and pellet injection. The limited data set with pellet fueling does not allow for a systematic comparison yet. One reason is that with the current setup pellet fueling is only possible transiently and the other reason is that, at least in this transient phase, the critical density is significantly higher than in plasmas with gas-fueling only. The few radiative collapses that have been observed in the transient phase overcame the critical density without pellet fueling by a factor of two to four [21]. This suggests that the density limit is, as assumed by the models, a local edge radiation limit rather than a global one. The impact of boronization was studied in much greater detail and the results are discussed in the following.

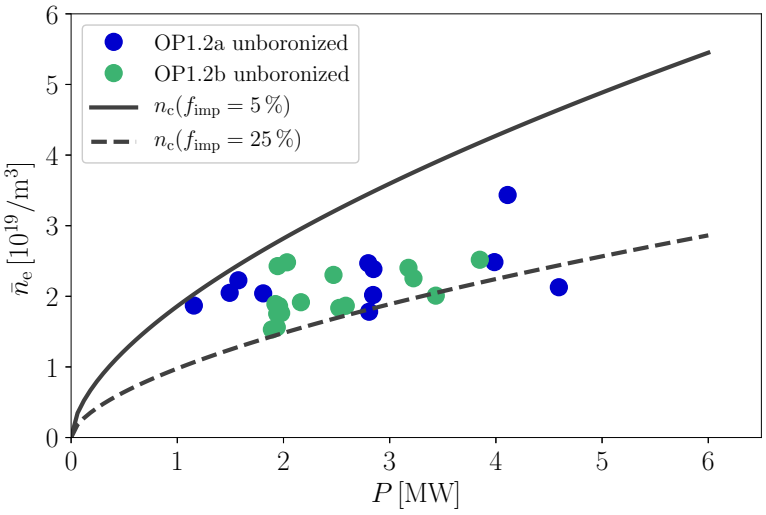

Figure 2: Line-averaged density and heating power of radiative collapses observed in W7-X before the first boronization together with two reference scalings for different impurity concentrations according to Eq. (6).

4.2 Operation with boronized walls

After boronization, spectroscopic diagnostics saw a significant decrease of carbon and oxygen radiation and no clear change in the low levels of high-Z impurity radiation. For carbon, the typical signal level was reduced to about one third, for oxygen a reduction by about one order of magnitude was observed [8]. Deriving changes in the impurity concentrations from the acquired data is still work in progress, but their significant reduction is clear already after the first boronization. Concurrently, radiative collapses appeared at higher densities, broadening the operational window. This is depicted in Fig. 3, where radiative collapses in experiments within two weeks after the first boronization (to ensure comparable conditions) are shown for three different magnetic configurations (standard, high-iota and high-mirror). As a reference, the critical density for the standard configuration is shown with an assumed reduction of the impurity concentration by a factor of about ten ($f_{\mathrm{imp}} = 0.5$).

It can be seen that, based on Eq. (6), the empirical critical density is compatible with the assumed reduction and indeed no strong configuration dependence is observed. Furthermore, the power scaling of the critical density seems to be stronger than before boronization, following the predicted scaling more closely even at higher powers (cf. Fig. 2). At least part of the reason is a changing profile shape. This is shown in Fig. 4, where the line-averaged

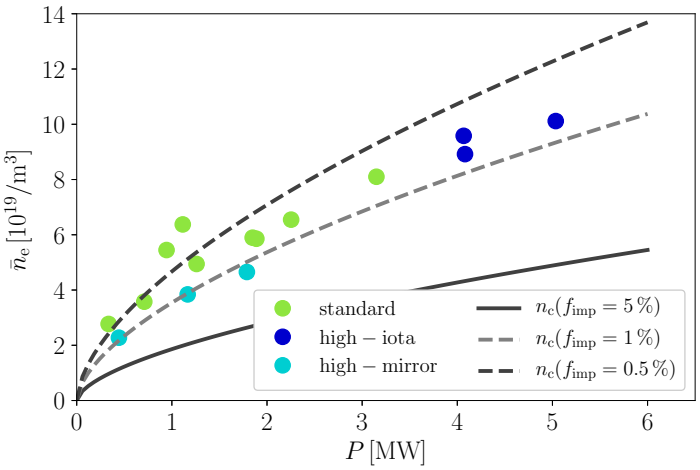

Figure 3: Line-averaged electron density and heating power of radiative collapses observed in different magnetic configurations in the two weeks after the first boronization. For reference, $n_c(f_{imp} = 4\,\%)$ (before boronization) and $n_c(f_{imp} = 0.5\,\%)$ are shown.

density was divided by a shape factor δ, defined as the ratio of the central electron density and the one at 85 % of the minor radius. The required electron density profiles were measured by the Thomson scattering diagnostic at W7-X. So far, the definition of δ has been chosen arbitrarily to represent the edge density. A systematic comparison of different radial locations is a subject of further research. Nevertheless, it was found that with this proxy for the edge density a lower scatter is observed compared to the line-averaged density and at the same time the power scaling is stronger and closer to the $P^{0.6}$-dependence predicted by Eq. (6), which indicates that the radiative density limit at W7-X could indeed be an edge density limit. This is in good agreement with similar observations from LHD [22]. Note that in the analyzed experiments the central density profiles are flat and, hence, δ does not represent profile peaking but rather describes the exact location of the edge density gradient.

Important open questions concern the role of local effects and whether the impurity concentrations assumed above reflect the actual impurity concentrations in the plasma (i. e. if the impurity concentration scaling of Eq. (6) indeed describes changes in the critical density). Nevertheless, it can be concluded that while the details may change drastically between limiter operation [23], unboronized and boronized divertor operation, the general phenomenology

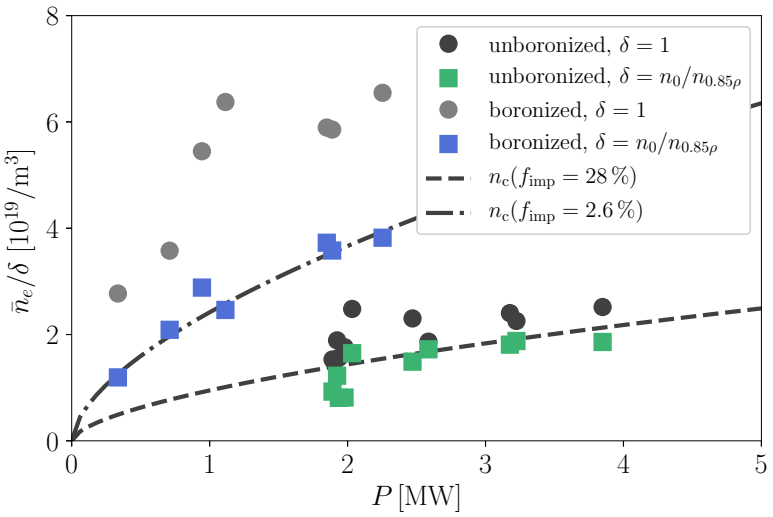

Figure 4: The critical density normalized by δ as a function of heating power before and after boronization. The circles indicate the case of $\delta = 1$ (completely flat density profile), while the squares account for a changing peaking of the density profile by defining δ as the ratio of the central density, n_0, and the density at 85 % of the minor radius, $n_{0.85\rho}$. The dashed lines indicate critical density scalings with $f_{\mathrm{imp}} = 20\,\%$ and 2.5 % respectively (as before, the absolute value of f_{imp} required to match the data depends on the choice of c_{rad}, see Sec. 3 for a detailed discussion).

of the radiative collapses remains the same. Furthermore, the current level of heating power is limiting the achievable density below the level targeted for the future (approximately 1 to $2 \cdot 10^{20}/\mathrm{m}^3$), but with the planned upgrades to 10 MW or beyond, these are expected to be achieved.

5 Density dependence of the global energy confinement

According to the empirical ISS04 scaling and neoclassical transport simulations [24], the energy confinement time of W7-X plasmas should increase with the density and degrade with power. This is, however, not necessarily true close to operational limits. In the limiter campaign, OP1.1, the energy confinement time showed a density scaling slightly stronger than ISS04. However, at low power the density was approaching the critical density and the density scaling became weaker. The reason is believed to be a pressure drop in the outer parts of the confined plasma induced by radiative losses [13]. As with the radiative collapses, it cannot be expected that the described confinement properties will be identical in divertor operation and with or without boronization. In the following the energy confinement time scaling in the first divertor experiments is presented before and after boronization. Special emphasis is put on determining whether confinement is degrading at high densities (i.e. a negative density scaling of τ_E is observed). So far, no strong differences have been seen between different magnetic configurations and, hence, for clarity only data from the standard configuration are shown. The data are selected from stationary phases where the density and stored energy change less than 10 % over one energy confinement time. Experimentally, the energy confinement time is calculated from the diamagnetic energy and the ECRH power as $\tau_\mathrm{E} = W_\mathrm{dia}/(P_\mathrm{ECRH} - \mathrm{d}W_\mathrm{dia}/\mathrm{d}t)$. In the analyzed plasmas, the ECRH was operated in X2-mode, where more than 95 % of the input power are absorbed and the effective heating power can be estimated by the ECRH input power P_ECRH. No correction for the radiation is performed. Since the analyzed plasmas show predominantly edge radiation, it does not seem justified to subtract the radiation power from the heating power.

As long as the magnetic configuration remains unchanged, the energy confinement time depends mainly on the density and the heating power (cf. Eq. (1)). In order to compare plasmas at different parameters, especially at densities that were not accessible before boronization, it is convenient to compare the so-called configuration factor, which is the average ratio of the energy confinement time and the ISS04 scaling ($f_\mathrm{r} = \langle \tau_\mathrm{E}/\tau_\mathrm{ISS04} \rangle$). Since

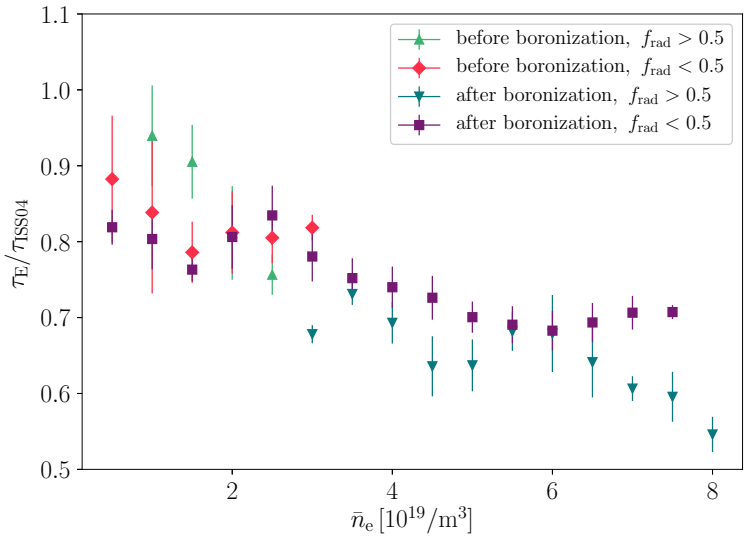

Figure 5: Energy confinement time normalized to ISS04 for the standard configuration, averaged for different densities before and after boronization. The data is shown separately for plasmas with P_{rad}/P_{ECRH} smaller and larger than 0.5 respectively. The individual data points represent the average value for density intervals of $\Delta n = 0.5 \cdot 10^{19}\,m^{-3}$ and the error bars represent the standard deviation in the respective interval.

ISS04 is an empirical scaling, observing an agreement or disagreement is not an instructive observation in itself. Normalizing the energy confinement time to $\tau_{\mathrm{ISS04}}\rangle$ is, however, a convenient way to identify and visualize trends in the scaling parameters of τ_{E}. In Fig. 5, the configuration factor is shown as a function of the line-averaged density. The individual data points represent f_{r} averaged in a density interval of $\Delta n = 0.5 \cdot 10^{19}\,\mathrm{m}^{-3}$ for stationary phases of the plasma and the error bars represent the standard deviation of f_{r} in the respective interval. This error represents changes in the machine conditions and deviations in the power degradation from ISS04. As will be shown below the power degradation observed in these experiments is relatively close to the one of ISS04, making f_{r} essentially a function of the density. Furthermore, the data set is shown separately for low and high radiated fractions ($f_{\mathrm{rad}} = P_{\mathrm{rad}}/P_{\mathrm{ECRH}}$) below and above 50 % respectively. Note that the estimation of the radiated power from the bolometer diagnostic requires assumptions concerning the spatial distribution of the radiation, especially concerning the toroidal asymmetry. Hence, the absolute value of P_{rad} may differ from the actual total radiation power. However, especially at higher values of the radiated fractions this effect is probably small [17]. Keeping this in mind, the following observations can be made: 1) The energy confinement time before and after boronization is essentially unchanged for densities that were accessible already before boronization. 2) The density scaling in both cases is weaker than suggested by ISS04 (otherwise f_{r} would be constant) and seems to change over the scanned density range: Especially for the low-radiation dataset, f_{r} is almost constant up until $3 \cdot 10^{19}\,\mathrm{m}^{-3}$, decreases strongly between 3 and $5 \cdot 10^{19}\,\mathrm{m}^{-3}$ and is almost constant again above $5 \cdot 10^{19}\,\mathrm{m}^{-3}$. 3) Of the two data sets, the one excluding high radiated fractions shows a stronger density scaling (closer to ISS04). This does not imply, however, that the radiation itself is impacting confinement. At low radiated fractions, for example, the global energy confinement seems to be almost unaffected by the level of radiation. The latter can be seen in Fig. 5 by comparing plasmas before and after boronization, which have basically identical confinement times and also from the weak density scaling between 3 and $5 \cdot 10^{19}\,\mathrm{m}^{-3}$ even at low levels of radiation. The reason for this behavior is still under investigation.

In Fig. 5, the data were sorted into "low" and "high" radiation plasmas (above and below $f_{\mathrm{r}} = 50\,\%$). The high-radiation plasmas showed, on average, a lower energy confinement than the low-radiation plasmas. In Fig. 6 it can be seen that this relative decrease in confinement is a gradual phenomenon, increasing with f_{rad}. The figure shows a comparison of experimental energy confinement times with the ISS04 scaling for plasmas after boronization, the color-code represents f_{rad}. It is obvious that the closest

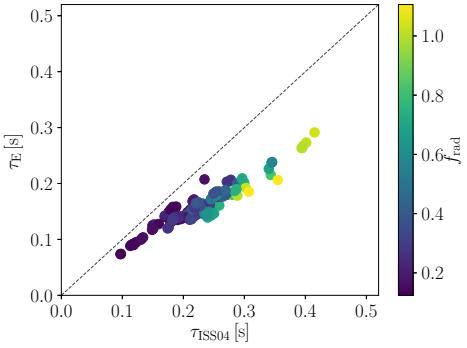

Figure 6: The energy confinement time, τ_E, is compared to the ISS04 prediction, τ_{ISS04}, at different radiated fractions f_{rad} (color-coded). With increasing f_{rad}, a clear deviation of τ_E from the ISS04 scaling is apparent. Every data point represents an average value over 200 ms of stationary plasma operation with changes in the stored energy, line-averaged density and heating power of less than 10 %.

match between τ_E and ISS04 is observed at the lowest values of f_{rad} up until 30 %. At higher values, $\langle \tau_E/\tau_{ISS04} \rangle$ starts to decrease gradually, being clearly reduced at an f_{rad} of about 70 %.

Since it is observed that, at constant density, f_{rad} increases with decreasing heating power, the results presented above indicate that the density dependence of the energy confinement should be strongest at low values of n_e/n_c. This is demonstrated in Fig. 7, where the scaling factors for density (n^α) and heating power (P^β) are depicted as a function of the line-averaged density normalized to the critical density before boronization $n_c(f_{imp} = 4\,\%)$ (averaged over intervals of $\Delta n_e/n_c = 0.5$). As expected, the data show the gradual weakening of the density dependence of τ_E with increasing n_e/n_c. The negative power scaling is almost constant and only weakens close to the collapse. It is still under investigation if this reflects changes in transport or is only caused by the fact that the collapse can be avoided by increasing the heating power. An actual confinement degradation (negative α) occurs only at the highest densities that can be achieved before a radiative collapse, indicating that indeed the radiative density limit not only narrows the accessible operational window, it also affects the energy confinement close to it. Nevertheless, even if the density dependence gets weaker, it is still beneficial for confinement to increase the density. The reason for the gradual weakening of the density scaling even at modest radiation levels is still under investigation and may be caused by coincident changes in trans-

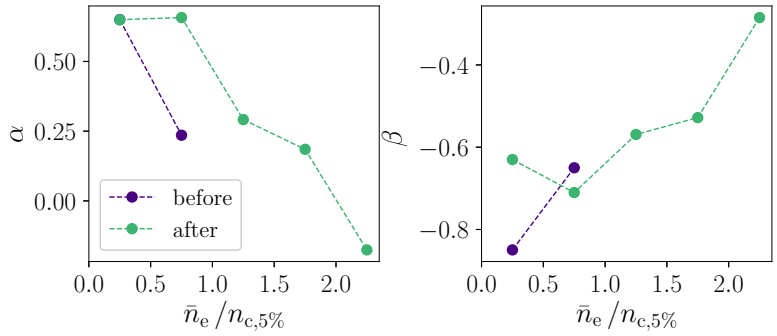

Figure 7: Scaling exponents for the density (α) and heating power (β) as a function of the line-averaged density normalized to $n_c(f_{imp} = 4\,\%)$ before and after boronization. The dashed lines are only shown to guide the eye.

port and fueling efficiency. It is interesting to note that a weakening of the density scaling of τ_E at higher densities is also observed in other stellarators, e. g. in LHD [25] and W7-AS [26].

6 Summary and conclusion

One of the key advantages of the stellarator concept for fusion energy production is the ability to go to high density, which, among other benefits, increases the energy confinement time for a given heating power. W7-X has only started to explore high density operation. Before boronization, the operational window was severely limited by radiative collapses believed to be caused by edge impurity radiation. Scaling laws derived from simplified analytical models are able to roughly predict the power-dependent critical density for these collapses, although many open questions concerning the exact cause and dynamics of these collapses remain. After boronization, the critical density was increased by a factor of two to three, for all the magnetic configurations that were investigated. Even higher densities were achieved when pellet injection was used to fuel the plasma - up to a factor of four above the earlier limit. These two observations are consistent with the conclusion that the W7-X density limit is due to edge radiation. For the plasmas analyzed in this study, a positive scaling of the energy confinement time with density was confirmed. For plasmas with low radiative losses, the density scaling follows roughly the empirical ISS04 scaling for stellarators and a configuration factor $f_r = \tau_E/\tau_{ISS04}$ between 0.7 and 0.8 is observed (note that $f_r = 1$ is comparable to a tokamak H-factor of approximately 1, i. e. the lower range of tokamak H-mode confinement [27]). At higher radiated fractions, the density

dependence becomes weaker. However, only at the highest densities, close to the collapse, does the stored energy start to degrade. Understanding why the observed density scaling is getting weaker at higher densities is work in progress. An obvious speculation is that due to the neoclassical optimization the importance of turbulent transport is increased. In the limiter phase of W7-X this was most likely the case [13, 27].

An important question for the future of W7-X is of course how the confinement can be improved even further. If the main cause for the weaker density scaling at higher densities is indeed impurity radiation from the edge plasma, reducing the intrinsic impurity content is important. This will be attempted by further improving the wall-conditioning methods, and by installing a steady-state pellet fueling system. Operation without carbon-based plasma-facing wall components could also help, but may require additional injection of light impurities in order to increase radiation for mitigating heat-loads and possibly facilitating detachment. In fact, investigating stellarator performance with a full-metal wall is a key issue for the future stellarator research. More heating power will be beneficial as well, both by increasing the achievable density, and also by raising the core ion temperatures to the 4 to 7 keV range where the effects of the neoclassical optimization will be more obvious. Finally, since confinement is and presumably will continue to be limited by turbulent transport, development of improved confinement regimes with suppression of turbulent transport will be important, and more heating power could provide access to H-mode-like operational regimes.

The results presented in this paper indicate that the development of steady-state regimes will have to consider the fact that the radiative density limit sets a boundary to the operational space of W7-X, but also that the target densities can indeed be achieved with sufficient heating power.

Acknowledgment

This work has been carried out within the framework of the EUROfusion Consortium and has received funding from the Euratom research and training program 2014-2018 and 2019-2020 under grant agreement No 633053. The views and opinions expressed herein do not necessarily reflect those of the European Commision.

References

[1] H. Yamada et al., *Nucl. Fusion* **45**, (2005) 1684

[2] A. Komori et al., *Fusion Sci. Technol.* **58**, (2010) 1

[3] R.C. Wolf, C.D. Beidler, A. Dinklage, P. Helander, H.P. Laqua, F. Schauer, T. Sunn Pedersen, F. Warmer, and Wendelstein 7-X Team, *IEEE Trans. Plasma Sci.* **44**, (2016) 1466

[4] T. Klinger et al., *Plasma Phys. Control. Fusion* **59**, (2017) 014018

[5] T. Sunn Pedersen et al., *Phys. Plasmas* **24**, (2017) 055503

[6] R.C. Wolf et al., *Nucl. Fusion* **57**, (2017) 102020

[7] T. Klinger et al., *Nucl. Fusion* **59**, (2019) 112004

[8] T. Sunn Pedersen et al., *Nucl. Fusion* **59**, (2019) 096014

[9] H. Wobig, *Plasma Phys. Control. Fusion* **42**, (2000) 931

[10] B. Lipschultz et al., *Nucl. Fusion* **24**, (1984) 977

[11] U. Wenzel et al., *Nucl. Fusion* **58**, (2018) 096025

[12] S. Sudo, Y. Takeiri, H. Zushi, F. Sano, K. Itoh, K. Kondo, and A. Iiyoshi, Nucl. Fusion **30**, (1990) 11

[13] G. Fuchert et al., *Nucl. Fusion* **58**, (2018) 106029

[14] K. Itoh and S.-I. Itoh, *J. Phys. Soc. Jpn.* **57** (1988) 1269-1272

[15] L. Giannone et al., *Plasma Phys. Control. Fusion* **45** (2003) 1713

[16] P. Zanca, F. Sattin, D. F. Escande, G. Pucella, and O. Tudisco, Nucl. Fusion **57**, (2017) 056010

[17] D. Zhang et al., *Phys. Rev. Lett.* **123**, (2019) 025002

[18] M. Hirsch et al., *Plasma Phys. Control. Fusion* **50**, (2008) 053001

[19] J. Geiger et al., *Plasma Phys. Control. Fusion* **57**, (2015) 014004

[20] D. Zhang, R. Burhenn, R. König, L. Giannone, P.A. Grodzki, B. Klein, K. Grosser, J. Baldzuhn, K. Ewert, V. Erckmann, M. Hirsch, H.P. Laqua, and J.W. Oosterbeek, *Rev. Sci. Instrum.* **81**, (2010) 10E134

[21] J. Baldzuhn et al., *Plasma Phys. Control. Fusion* **61**, (2019) 095012

[22] J. Miyazawa et al., *Nucl. Fusion* **48**, (2008) 015003

[23] G. Fuchert et al., *Proc. 23 Europ. Conf. on Circuit Theory and Design (2017, Catania, Italy)*, IEEE, NY (2017)

[24] Y. Turkin, C. D. Beidler, H. Maßberg, S. Murakami, V. Tribaldos, and A. Wakasa, *Phys. Plasmas* **18**, (2011) 022505

[25] H. Yamada et al., *Plasma Phys. Control. Fusion* **49**, (2007) B487

[26] U. Stroth, *Plasma Phys. Control. Fusion* **40**, (1998) 9

[27] A. Dinklage et al., *Nat. Phys.* **14**, (2018) 855-860